Design and Analysis of Lattice Structures for Additive Manufacturing

Christiane Beyer[1]
Mem. ASME
Associate Professor
California State University Long Beach,
Mechanical and Aerospace Engineering,
1250 Bellflower Boulevard,
Long Beach, CA 90840
e-mail: chris.beyer@csulb.edu

Dustin Figueroa
Design Engineer
Fusion Formatics Corporation,
4398 Corporate Center Dr,
Los Alamitos, CA 90720
e-mail: dustin.figueroa@fusionformatics.com

Additive manufacturing (AM) enables time and cost savings in the product development process. It has great potential in the manufacturing of lighter parts or tools by the embedding of cellular/lattice structures that consume less material while still distributing the necessary strength. Less weight and less material consumption can lead to enormous energy and cost savings. Although AM has come a long way over the past 25–30 years since the first technology was invented, the design of parts and tools that capitalize on the technology do not yet encompass its full potential. Designing for AM requires departing from traditional design guidelines and adopting new design considerations and thought structures. Where previous manufacturing techniques (computer numerical control (CNC) machining, casting, etc.) often necessitated solid parts, AM allows for complex parts with cellular and lattice structure implementation. The lattice structure geometry can be manipulated to deliver the level of performance required of the part. The development and research of different cell and lattice structures for lightweight design is of significant interest for realizing the full potential of AM technologies. The research not only includes analysis of existing software tools to design and optimize cell structures, but it also involves design consideration of different unit cell structures. This paper gives a solid foundation of an experimental analysis of additive manufactured parts with diverse unit cell structures in compression and flexural tests. Although the research also includes theoretical finite element analysis (FEA) of the models, the results are not considered here. As an introduction, the paper briefly explains the basics of stress and strain relationship and summarizes the test procedure and methods. The tests concentrate primarily on the analysis of 3D printed polymer parts manufactured using PolyJet technology. The results show the behavior of test specimens with different cell structures under compression and bending load. However, the research has been extended and is still ongoing with an analysis of selective laser melted test specimens in aluminum alloy AlSi10Mg. [DOI: 10.1115/1.4033957]

Keywords: additive manufacturing, lattice structure design, unit cell, weight reduction, compressive test, flexural test

1 Introduction

Manufacturing constraints have long limited design engineers in their creativity. Truly optimal designs were not able to be produced; instead, they were replaced by designs that catered to the manufacturing abilities of the day. Recently, these manufacturing constraints have lifted significantly due to innovations in AM [1–7]. While some constraints remain (e.g., overhang and build size), parts can generally be made according to the design that best fulfills the part's function. Part of best fulfilling a required function is the effective use of all materials, or using as little material as necessary. This is especially true in the automotive and aerospace industry, where saving a seemingly insignificant amount of mass can translate to substantial cost reduction or performance increase [8]. For example, a 2008 study by Ricardo, Inc. [9] found that for every ten pounds removed from a gasoline-powered car, the vehicle's Environmental Protection Agency (EPA) combined fuel economy increased by 0.15%. Weight reduction is even more important in aerospace, where each kilogram can cost around $10,000 [10]. Therefore, a great demand for functional parts manufactured with minimal material exists. Lattice structures can help to accomplish this goal.

A lattice consists of a pattern repeated regularly in all directions. This pattern is known as a unit cell. Because the unit cell is not solid material, the lattice structure has less mass per volume than the solid part. While the lattice is inherently weaker than a solid part of the same dimensions, a proper knowledge of the properties of lattice structures may validate their future integration in design. However, before these advancements in design can be made, the relationship between lattice parameters and properties must be understood.

Numerous resources summarize the current understanding of the cell structures and their mechanical behavior [11–19]. Other sources demonstrate the design and verification of cellular structures for special application from the design to fabrication and testing [20–27]. Additional effort focuses on the development of special geometric methods and software tools to efficiently create computer-aided design (CAD) models of cellular unit cells and lightweight truss structures as well as optimizing the structures to achieve superior strength, stiffness, and weight characteristics [28–31].

Reference [13] describes that the three major factors influencing the properties of cellular structures are (1) the properties of the material, (2) the topology and shape of the cell, and (3) the relative density of the cellular structure. The objective of this research is to explore different unit cells structures and their compressive and flexural properties. Basic compressive and flexural (or bend) tests are utilized to experimentally determine these characteristics. The ultimate goal is to build enough of an understanding of unit cell properties to effectively and efficiently replace solid parts with lattice structures and create new parts utilizing lattice structures to their full potential.

2 Background

Two tests were used to analyze the properties of various lattice geometries, compression and flexure tests. These tests were

[1]Corresponding author.

Manuscript received October 5, 2015; final manuscript received June 7, 2016; published online September 29, 2016. Assoc. Editor: Z. J. Pei.

modeled after the ASTM standards developed for solid structures. More details will be provided in Sec. 3. All axes and reference directions for both compression and flexing specimens are defined in Figs. 1 and 2.

The concepts utilized in the following research are relatively simple and do not involve complicated calculation. Only a basic knowledge of the mechanics of materials is required to derive the necessary equations.

The first definition required the calculation of engineering stress, represented by

$$\text{Engineering Stress } \sigma = \frac{F}{A} \tag{1}$$

Sigma represents the engineering stress (simply referred to as stress), F is the load applied to the specimen, and A is the initial cross-sectional area normal to the direction of the force [32].

The second definition required the calculation of engineering strain, represented by

$$\text{Engineering Strain } \varepsilon = \frac{\Delta l}{l_o} \tag{2}$$

Epsilon is the engineering strain, Δl is the linear deformation from the initial position along a defined direction, and l_o is the initial length in the same defined direction. In this paper, the defined direction is assumed to be the direction of the compression [32].

The maximum stress found in a solid specimen undergoing a four-point bending test needed to be derived. Figure 3 [33] shows the free body diagram for the test setup with the related following equation:

$$\text{Moment of Middle Span (see Fig. 3) } M_{\text{midspan}} = \frac{Pa}{2} \tag{3}$$

$$\text{Maximum Flexural Stress } \sigma_{\max} = \frac{M_{\text{midspan}} \frac{h}{2}}{I} \tag{4}$$

In these equations, M_{midspan} is the moment present between the two central supports, $\sigma_{\max}$ is the largest stress present within the bar due to flex, and P represents the total force applied to the bar. The distance along the x-direction between the stationary support and displacing support is denoted a. The height of the bar in the z-direction was given by h. Finally, I is the moment of inertia about the axis perpendicular to the neutral axis and in the y-direction, which for the bar is $I = bh^3/12$ [32]. Here b represents the length in the y-direction. After substituting Eq. (3) into Eq. (4), following equation is derived giving stress in terms of force, as shown below

$$\text{Maximum Flexural Stress for 4Pt. Flex Test } \sigma_{\max} = \frac{3Pa}{bh^2} \tag{5}$$

The stress and strain information is utilized to create a stress–strain plot. From these plots, several properties useful to this research can be determined. These include yield stress, the modulus of elasticity, and flexural strength.

Yield stress (also known as yield strength) is the stress at which a material will transition from behaving elastically to plastically. It is typically determined using the 0.2% offset technique [32] discussed in more detail in Sec. 4.2.1.

The modulus of elasticity is the ratio of stress to strain while the material behaves elastically. This is graphically represented by the slope of the linear portion of the stress–strain curve (see Fig. 4) [34]. The higher the elastic modulus, the stiffer is the material [32]. The definitions discussed are labeled in a sample stress–strain curve shown below (see Fig. 4), where E represents the elastic modulus, $\sigma_{0.2\%\text{ys}}$ is the yield strength calculated using a 0.2% offset technique, σ_E is the engineering stress, and ε is the engineering strain.

The flexural strength of material is defined as the maximum stress occurring in a specimen during a flexural test [35]. This property is used to analyze the bend test results. To analyze the lattice structure geometries and determine their properties with respect to the amount of material used, relative analysis is used. This analysis consists of comparing the relative density of a lattice structure with the relative property of the structure. The relative density is represented by

$$\text{Relative Density } \rho_r = \frac{\rho_l}{\rho_s} \tag{6}$$

The relative density is ρ_r. The density of the lattice structure (ratio of mass of structure divided by volume structure would occupy if it were solid) is given by ρ_l. Finally, ρ_s represents the density of the solid material. Knowing the relative density allows for a better assessment of the performance of a lattice structure.

Similarly to relative density, a general relative property is defined as

$$\text{General Relative Property } P_r = \frac{P_l}{P_s} \tag{7}$$

Here P_r is the relative property, P_l is the property of the lattice structure calculated with the assumption that the structure was solid, and P_s is the solid material property [33]. This general form is applied to both yield strength and flexural strength in the analysis.

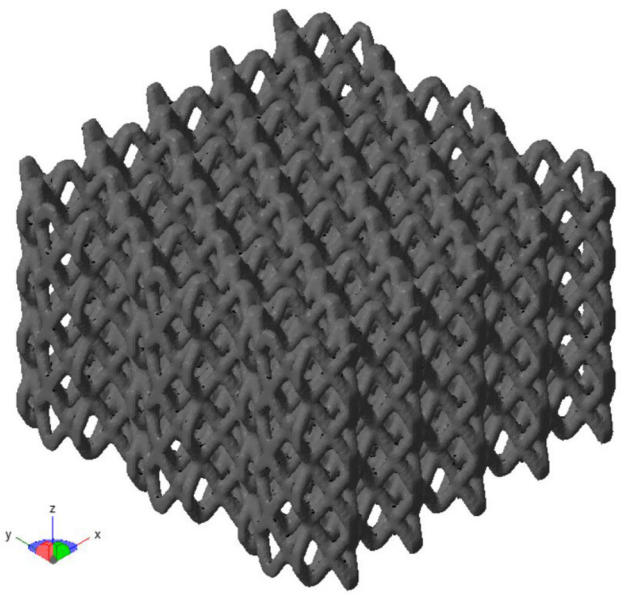

Fig. 1 Axis definitions for compression tests

3 Methods

3.1 Design and Manufacture. All specimens with the diverse unit cell structures were developed utilizing NETFABB[1] SELECTIVE SPACE STRUCTURES (3S), a software tool which enables turning solid parts into advanced structures. It facilitates the creation of the individual unit cell geometries, a combination of bars, surface elements or solid models, and their application in the overall structure [36]. In our research, a rectangular prism for compression tests and a bar for flexure testing with different cell structures were created. Specific dimensions and figures of the specimens are given in Secs. 4 and 5.1. The geometries were exported as STL (STereoLithography; sometimes also referred to as Standard Triangle Language or Standard Tessellation

[1]Software named AUTODESK NETFABB since Autodesk acquired Netfabb in September 2015.

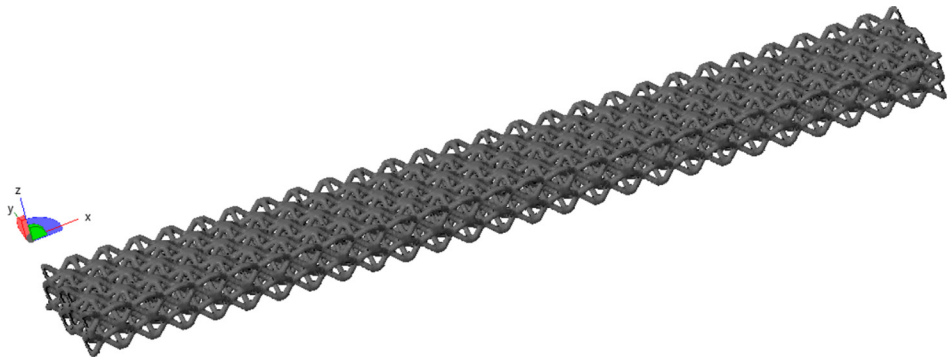

Fig. 2 Axis definitions for flexure tests

Language) files, a file format which describes the surface geometry of a three-dimensional object with unstructured triangulated flat facets [37]. Because of the high number of cell structures, the CAD models have an increased surface area. For a high resolution and suitable printing tolerances, a high number of triangular facets are necessary, which result in memory intensive STL files. A better option in the future is the usage of the newly developed additive manufacturing file (AMF) format, which describes the same surface area with fewer triangles by using curved facets [38]. Additional potential lies in the development of new algorithms and methods for data formats. The so-termed modified boundary octree data structure algorithm is used to convert the STL file of an object to an octree data structure based on the part's geometry, the machine parameters, and a user-defined tolerance value [39].

For AM, PolyJet technology [24,40] has been used with an Objet30 3D printer [41] from formerly Objet Geometries, Ltd., which merged in 2011 with Stratasys. The PolyJet technology is a method that produces smooth, very complex, and accurate parts by jetting droplets of curable liquid photopolymer with a 16 μm layer resolution and accuracy as high as 0.1 mm onto a build tray. UV lamps instantly cure the tiny droplets of liquid photopolymer. Overhangs or complex shapes are supported by a removable gel-like support material which is simultaneously applied with the model material in jetting droplets to the build tray. The support materials can easily be removed with a water jet stream. As model material, the polymer VeroWhitePlus was used with the given material properties shown in Table 1 [42].

The sophisticated, embedded build-preparation software OBJET STUDIO automatically calculates from a 3D CAD file the placement of parts on the build platform as well as usage of photopolymers and support material. The cubical compression geometries were printed with the z-axis perpendicular to the print bed. For the bending bars, the x–y plane was parallel to the print bed.

While the polymer specimens in this research were used to demonstrate a trend to the behavior of different cell structures, the goal was to confirm a nearly similar behavior with selective laser melted aluminum parts fabricated by Citim AM using an SLM 280 machine. The selective laser melting process uses high-powered, multilaser beam technology to create three-dimensional metal parts by fusing fine metal powders together [43,44]. The whole process is carried out under an inert gas atmosphere. In this research, the aluminum alloy AlSi10Mg has been used. With a density of 2.7 g/cm^3, aluminum is classified as a light metal [45]. It is highly suited to processing and is used, for example, in thin-walled components with complex geometries. AlSi10Mg is currently the most common alloy used in AM. In alloyed forms with additions as silicon, magnesium, copper or manganese, aluminum is used to produce components with high strength and high dynamic loadability, optimal for use in aerospace and automotive industry. Aluminum alloy components exhibit a homogeneous, near-zero porosity texture, whereby the mechanical characteristic values lie within the range of the material specifications. Through subsequent post treatment, such as hardening, heat treatment, or hot isostatic pressing, the components' properties can be adapted to meet specific requirements. The material properties of

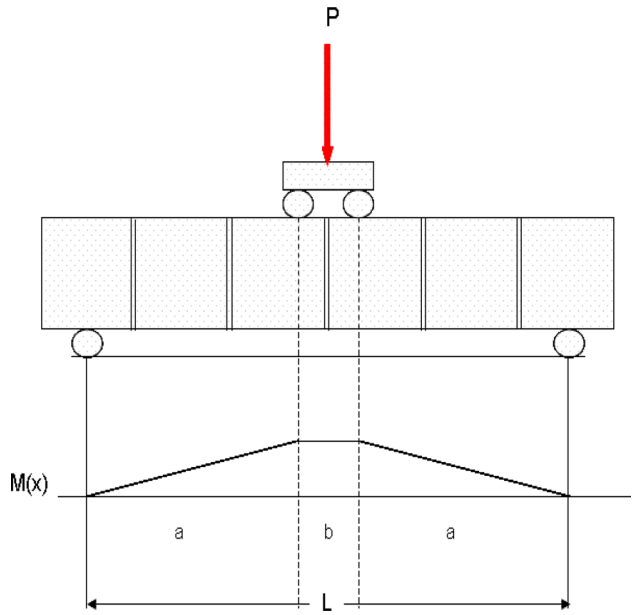

Fig. 3 Free body diagram for Four Pt Flex test [33]

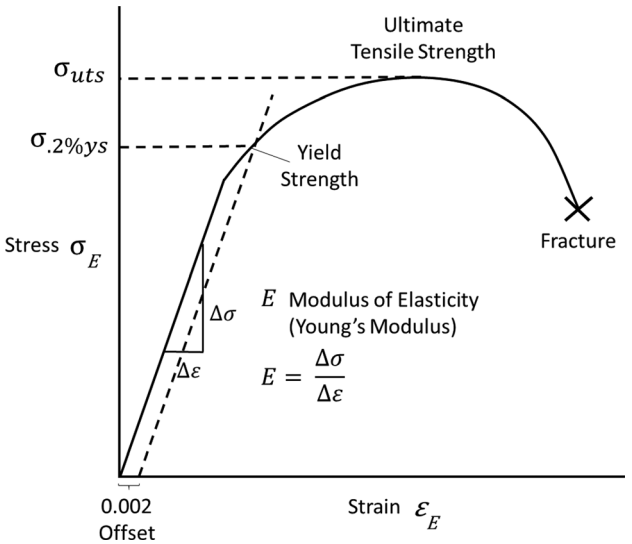

Fig. 4 Example of engineering stress–strain curve (adapted from Ref. [34])

Table 1 Material properties of the polymer VeroWhitePlus RDG835 [42]

Mechanical properties	ASTM	Units	Metric	Units	Imperial
Tensile strength	D-638-03	MPa	50–65	psi	7250–9450
Elongation at break	D-638-05	%	10–25	%	10–25
Modulus of elasticity	D-638-04	MPa	2000–3000	psi	290,000–435,000
Flexural strength	D-790-03	MPa	75–110	psi	11,000–16,000
Flexural modulus	D-790-04	MPa	2200–3200	psi	320,000–465,000
HDT (°C at@ 0.45 MPa	D-648-06	°C	45–50	°F	113–122
HDT °C at 1.82 MPa	D-648-07	°C	45–50	°(F	113—122
lzod notched impact	D-256-06	J/m	20–30	ft lb/in.	0.375–0.562
Water absorption	D-570-98 24 h	%	1.1–1.5	%	1.1–1.5
Tg	DMA, E»	°C	52–54	°F	126–129
Shore hardness (D)	Scale D	Scale D	83–86	Scale D	83–86
Rockwell hardness	Scale M	Scale M	73–76	Scale M	73–76
Polymerized density	ASTM D792	g/cm^3	1.17–1.18		

Table 2 Material properties of the aluminum alloy AlSi10Mg; layer thickness 50 μm, not heat treated [45]

Mechanical data	Symbol and Unit	AlSi10Mg (as built)
Tensile strength	Rm (MPa)	397 ± 11
Offset yield stress	Rp0,2 (MPa)	227 ± 11
Break strain	A (%)	6 ± 1
Reduction of area	Z (%)	8 ± 1
E-Modulus	E (GPa)	64 ± 10
Hardness by Vickers	(HV10)	117 ± 1
Surface roughness	Ra (μm)	7 ± 1
Surface roughness	Rz (μm)	46 ± 8

AlSi10Mg, built with layer thickness 50 μm, are shown in Table 2 [45].

Due to cost constraints, the metal compression cubes were not all printed in the same direction. In order for all cubes to print on a single print bed, some had to be rotated 90 deg so that the compression axis was parallel to the print bed. The orientation of the piece resulted in two different yield strengths. Data presented in this paper are the result of a single test unless otherwise specified. Only one sample of each unique structure was tested to see relative properties.

3.2 Compression Tests. All compression testing was carried out on an Instron 8502. The tests were constructed to replicate the ASTM standards as closely as possible. However, some modifications had to be made due to the nonuniformity of the surfaces of the structures. The compression tests were done according to ASTM D695. The machine was set up so that the cubes rested on one compression plate while another applied the compressive force from the top. The ramp rate of the machine was set to 0.05 in./min, while the data rate was 10 points/s. The tests were run until the force decreased with increasing displacement. Data were exported and analyzed in Microsoft Excel. An example of the test is shown in Fig. 5.

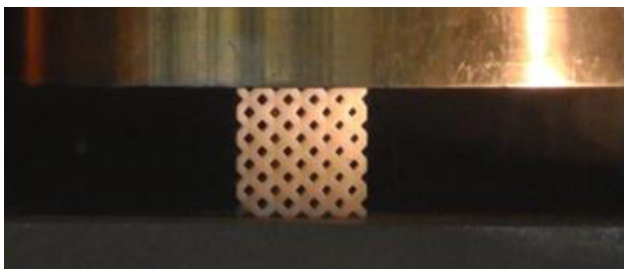

Fig. 5 Compression test setup

3.3 Flexure Tests. All flexure tests were also carried out on an Instron 8502 machine. This test was meant to replicate ASTM D790, a three-point bend test utilizing rounded supports. However, because the surface of the lattice geometries was not uniform but instead had peaks and valleys, the proper span distance could not be maintained. Therefore, the round supports were replaced with flat supports that were able to rotate to maintain tangency with the surface (see Fig. 6). To preserve consistency, the point of force application was replaced with a 1 in. wide flat surface as well. An adjustable rig was used to place the supports at the proper distance. Accuracy was verified at ±0.01 in. The machine ramp rate was 0.05 in./s, while the data rate was 10 points/s. Data were collected until the force decreased with increasing displacement, exported, and analyzed in Microsoft Excel.

4 First Test Series

4.1 Development of Unit Cell Structures and Specimen. The first group of specimens contained eight unique lattice unit cells. These lattice structures were carefully selected based on naturally occurring geometries and previously researched structures. Each unit cell was implemented in a cubic volume with 25 mm sides for compression testing according to ASTM D695. For flexural testing according to ASTM D790, bars were designed with dimensions of 225 mm × 25 mm × 13 mm. All specimens were designed with 2 mm diameter trusses and were printed on the Objet30 with the print bed parallel to the x–y plane. A summary of specimen data can be found in Tables 3 and 4.

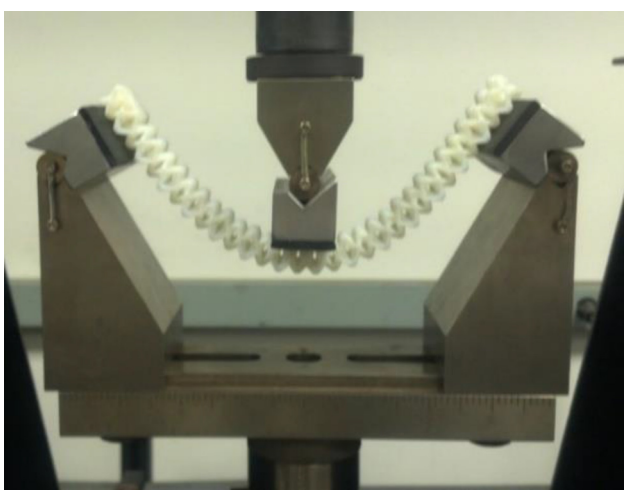

Fig. 6 Flexure test setup

Table 3 First series compression geometries

Name	Unit structure	Unit cell dimensions (mm)			Cube dimensions (mm)			Compression face area (mm^2)	Relative density (Netfabb)
		x	*y*	*z*	*x*	*y*	*z*		
C01		5.00	5.00	5.00	25.07	25.00	24.90	626.75	0.25
C02		6.25	6.25	6.25	25.03	25.00	24.90	625.75	0.49
C03		5.00	5.00	5.00	25.03	25.00	24.90	625.75	0.49
C04		5.00	5.00	5.00	25.03	24.99	24.90	625.50	0.63
H01		6.25	6.25	6.25	25.01	25.00	24.90	625.25	0.36
H02		6.25	7.23	6.25	25.01	25.00	24.90	625.25	0.53
H03		4.33	7.50	5.00	25.05	24.98	24.88	625.75	0.43
H04		14.43	8.33	12.50	24.04	24.99	24.81	600.76	0.26
Solid		—	—	—	25.00	25.00	25.00	625.00	1.00

Unit cell geometries are named according to the structures on which they are based. Structures based on rectangular prism geometries were designated by a "C" followed by the individual numeric designation of the cell. This number served only to differentiate unique lattice structures; it did not represent any information pertaining to the cell. Cells based on a hexagonal structure were designated with an "H." Once again, the numeric value following the letter only served to differentiate cells. Cells with a "b" following the name were designed for ASTM D790 (flex) testing, and therefore had to fulfill certain geometric constraints. Some unit cells were slightly scaled to better fit the ASTM requirements.

Cell C01 was developed to serve as a benchmark. It is a simple structure, consisting of bars on all edges of the cell. Cell C02 was developed to replicate the face centered cubic unit cell encountered in metal molecular lattices. This structure has nodes at all corners in addition to the center of all faces. The result can best be understood as C01 with an X on all faces, hollow on the inside. Cell C03 is a pyramidal structure developed from external research conducted on sandwich panel structures. Wadley [15] tested several lattice structures as a sandwich panel filler, including pyramidal, honeycomb, and tetragonal geometries. The authors found that pyramidal lattice structures were not as strong or stiff as honeycomb structures. However, due to the pyramidal structures' practical multidirectional effectiveness, they were selected here for analysis. The structure consists of four bars, each departing a corner of the bottom face, traveling through the center of the cell, then continuing on to the opposite corner of the top face. C04 was developed to replicate the body centered cubic cell structure encountered in materials science. The structure consisted of a combination of C01 and C03. Figure 7 shows all four discussed unit cells.

H01 represented a basic variation of the standard honeycomb cell. The central hexagon was stretched to allow the cell to be cubic. The top and bottom faces were identical, with bars connecting the corresponding nodes from top and bottom faces. H02 represented a traditional honeycomb pattern. The central hexagon was regular, and the resulting cell dimensions were not cubic. Similar to H01, the top and bottom faces were identical. Corresponding nodes from top and bottom faces were connected. H03 utilized a different unit cell to obtain an outcome similar to H02. The cell represented a regular hexagonal honeycomb with a larger diameter than H02. Finally, H04 was developed from the same sandwich panel research as C03, where its tetragonal geometry was found to be comparable to pyramidal lattices [14]. This design geometry resulted in a directional dependence. However, it was anticipated to be slightly stronger per unit mass than C03 and also was printable with current restrictions on metal AM. Therefore, it was selected as the last test unit cell in the first test series. Figure 8 shows all four hexagonal unit cells.

The designed unit cells have been implemented in the cubes for compression test and the bars for flexural test. Figure 9 shows the CAD models of all eight compression test cubes based on the

Table 4 First series flexure geometries

Name	Unit structure	Unit cell dimensions (mm)			Bar dimensions (mm)			Support–support distance (mm)	Relative density (Netfabb)
		x	*y*	*z*	*x*	*y*	*z*		
C01b		6.25	6.25	6.25	225.40	25.00	12.50	87.30	0.16
C02b		6.25	6.25	6.25	225.40	25.00	12.50	87.30	0.50
C03b		6.25	6.25	6.25	225.40	25.00	12.50	87.30	0.35
C04b		6.25	6.25	6.25	225.40	25.00	12.50	87.30	0.45
H01b		6.25	6.25	6.25	225.40	25.00	12.50	87.30	0.35
H02b		6.25	7.23	6.25	225.40	25.00	12.50	87.30	0.56
H03b		5.41	9.38	6.25	225.40	25.00	12.50	87.30	0.28
H04b		14.43	8.33	1.25	225.40	25.00	12.50	87.30	0.27

different unit cell structures. The CAD models of the eight specimens for the flexural test are not shown due to lack of space.

A summary of the characteristics of the various unit cells and structures can be found in Tables 3 and 4. For clarification, the support to support distance column of Table 4 refers to the distance between stationary supports and the edge of the displacing support (see Fig. 3).

4.2 Test Results and Calculation. The testing was carried out as described in Sec. 3. Due to the volume of data (thousands of points per specimen), the raw data have not been included in this publication. Instead, the processes used to refine the data into useful information are detailed in the remainder of this section.

The main goal of the research was to observe the relative properties of each lattice compared to its relative density. Therefore, the value of the selected property for the solid material had to be known (see Table 1). The availability of information dictated that the flexural strength is the comparative property for flexure tests, and the compressive yield strength is the comparative property chosen for compression testing. Unfortunately, not all relevant

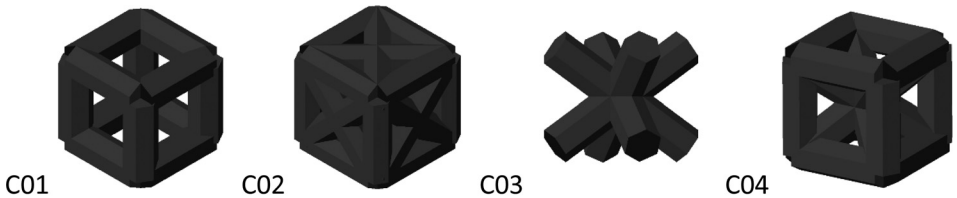

Fig. 7 Unit cells based on rectangular prism C01–C04

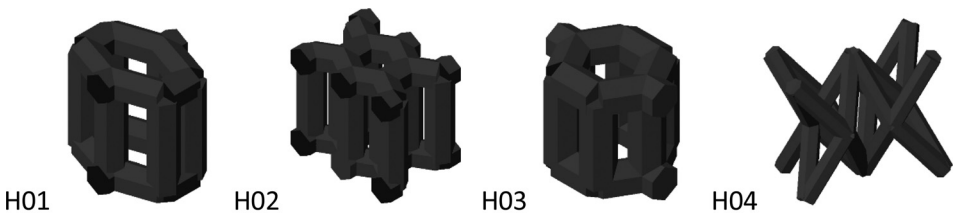

Fig. 8 Unit cells based on hexagonal structures H01–H04

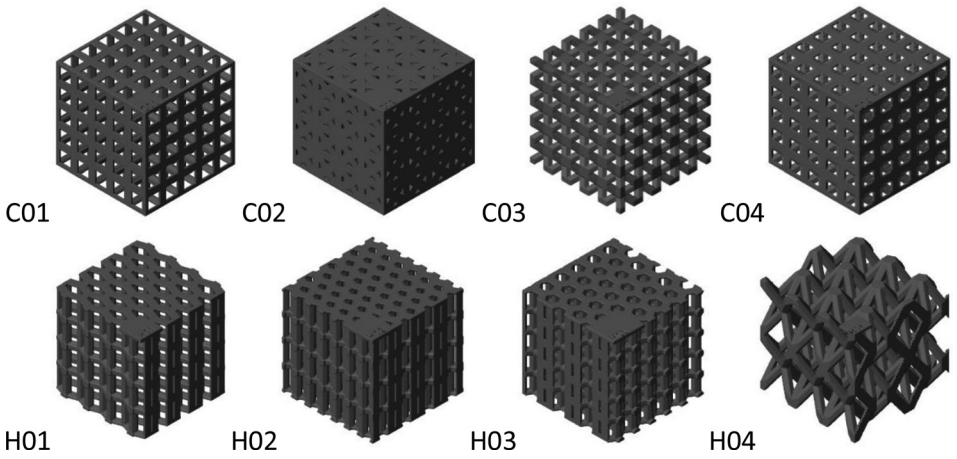

Fig. 9 Compression test cubes based on rectangular prism C01–C04 and hexagonal structures H01–H04

information could be found. Therefore, the compressive yield strength is determined experimentally using the same techniques described below.

4.2.1 Compression. Once data were obtained from the Instron equipment, they were imported to Excel for analysis. After converting the displacement and force from units of inches and pounds to meters and Newton, the stress was calculated using Eq. (1). The relevant force is the measured force (N) from the Instron machine. The surface area (mm^2) is the area of the faces normal to the compression ($-z$) direction. The strain was calculated using Eq. (2). The initial measurement is the initial dimension in the compression direction (mm). The change in length is the displacement measured from the Instron machine (converted to m). Once stress and strain for each data point had been calculated, they were plotted with strain as the abscissa and stress as the ordinate, as seen in Figs. 10 and 11.

These plots were analyzed within Excel and the equation of the linear portion (the elastic modulus) was found via linear regression between two points that best represented the elastic region (points determined by digitally enhanced visual inspection). Once the equation of the elastic region was found, a line of 0.2% offset was plotted along with the stress–strain curve. This line was determined using the following procedure. The equation of the trend line of the linear portion (elastic region) of the curve was assumed to be represented by $y = mx + b$, where y represented stress, x represented strain, m represented the elastic modulus, and b represented the y-intercept. From basic algebra, the equation of the line shifted 0.002 to the right is equal to $y_{\text{shifted}} = m(x - 0.002) + b$. Two points are needed to define the offset line. The first point is chosen to be the x-intercept, solved for as $x_{\text{int}} = (-b/m) + 0.002$. Therefore, the first point in the offset line is (x_{int}, 0). The strain value (x) for the calculation of the second point is needed only to surpass the maximum strain of the elastic region. The second point was calculated from the equation given above for y_{shifted}, and the offset line was plotted along with the original curve.

The point of intersection between the two curves was determined by digitally enhanced visual inspection. This value was chosen to be the yield strength of the geometry, with an anticipated error of ±0.05 MPa. The stress–strain plots of all geometries with 0.2% offset included are shown in Figs. 10 and 11.

For the experimental calculation of the solid compressive yield strength of the polymer, two solid cubes were created with the dimensions given in Table 3. The above procedure was followed with the exception of the calculation of relative yield strength (diagram not shown), which resulted in two values, 62.8 MPa and 70.4 MPa. With the solid value known, the relative strength was finally determined using Eq. (7). Because the solid value was presented as a range, the relative yield strength calculation was performed for each extrema to yield a maximum and minimum relative strength (see Table 5). The relative density–relative strength relationship was then tabulated and plotted for efficient comparison in Fig. 12. The one-to-one ratio was also plotted to provide a visual representation of the solid material.

4.2.2 Flexure. The property to be compared to relative density for the flexure tests is the relative flexural strength. The procedure for determining the relative properties was very similar to that for the compression testing. The system was modeled as a

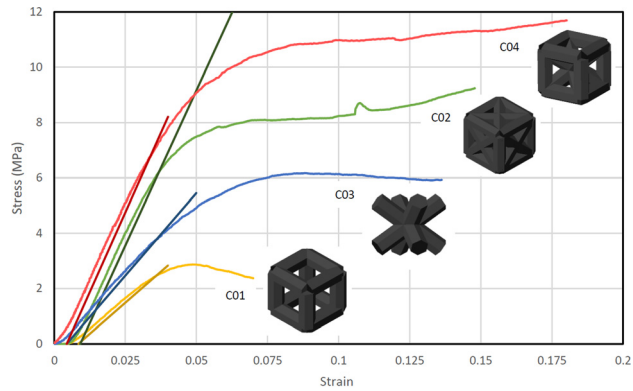

Fig. 10 Compression test results as stress–strain curve of cubes C01–C04 with offset curves

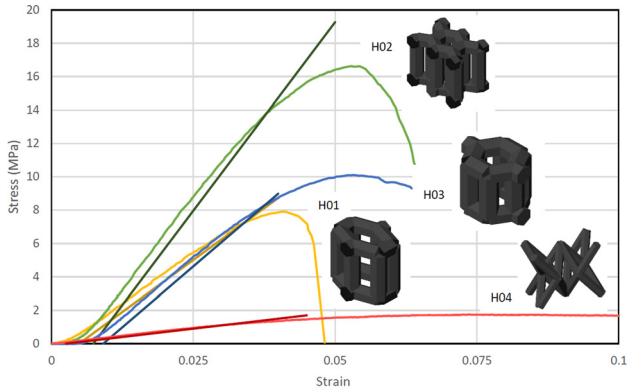

Fig. 11 Compression test results as stress–strain curve of cubes H01–H04 with offset curves

Table 5 Summary of results from first compression tests

Name	Unit structure	Relative density (Netfabb)	Yield strength (MPa)	Relative yield strength	
				Low	High
C01		0.25	2.49	0.035	0.040
C02		0.49	6.11	0.087	0.097
C03		0.49	3.82	0.054	0.061
C04		0.63	6.78	0.096	0.108
H01		0.36	7.25	0.103	0.115
H02		0.53	13.9	0.197	0.221
H03		0.43	8.24	0.117	0.131
H04		0.26	1.14	0.016	0.018
Solid		1.00	62.8–70.4	—	—

four-point flexure test chosen to better represent the flat support, which upon bar bending, maintained two lines of contact with the bar. Therefore, Eq. (5) was used to calculate the maximum flexural stress occurring within the structure.

Once the stress at each data point had been calculated, the maximum stress was found. This value represented the flexure strength. The relative flexural strength was then calculated via Eq. (7) (see Table 6). The value for the solid flexural strength was given from the material spec sheet in Table 1. The results were tabulated and graphed for quick comparison (see Fig. 13).

4.3 Analysis of First Test Series Results. While the results obtained did help to edify an understanding between lattice structure form and properties, several overlooked factors reduced the effectiveness of the results. The acquired data supported the established premise that hexagonal cells have relatively superior compressive properties [46]. As seen in Figs. 12 and 13, the hexagon-based unit cells (designated by H in the name) were consistently closer to the one-to-one ratio than their cubic counterparts. The exception to this trend was C01, which performed surprisingly well for its low relative density and simple unit cell structure. A unifying feature of the cells that returned results close to the one-to-one ratio was their incorporation of trusses in the *z*-direction. Knowing that each of these cells is a bend-dominated structure [47], the vertical trusses along the *z*-direction may have produced a smaller moment about the nodes relative to unit cells lacking trusses in the z-direction. However, when the moment became significant enough to angularly displace the vertical trusses, dramatic deformation ensued. This relatively rapid failure mode may be the cause of the clear peak stresses present in cells containing trusses in the z-direction, followed by reduced stresses once failure had occurred (see Figs. 10 and 11). Cells lacking trusses in the *z*-direction experienced a gradual stress plateau instead of a decline. H04 is an exception to this trend, but it should not be given much consideration for reasons discussed later in this section. This hypothesis is also supported by examining the structure of C03, which is essentially C01 with a translated and rotated frame of reference. When the compressive results from C01 and C03 are compared (see Fig. 12), it is clear that C01 produced

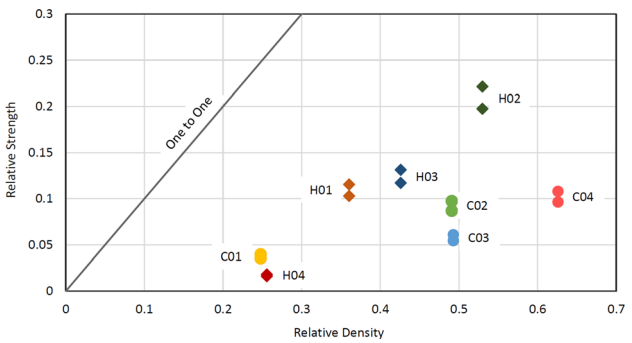

Fig. 12 Summary of results from first compression tests

Table 6 Summary of results from first flexure tests

Name	Unit structure	Relative density (Netfabb)	Flexural strength (MPa)	Relative flexural strength	
				Low	High
C01b		0.16	1.56	0.014	0.021
C02b		0.50	8.91	0.081	0.119
C03b		0.35	1.84	0.017	0.025
C04b		0.45	5.35	0.049	0.071
H01b		0.35	1.40	0.013	0.019
H02b		0.56	4.54	0.041	0.061
H03b		0.28	1.99	0.018	0.027
H04b		0.27	0.58	0.005	0.008
Solid		1.00	75–110	—	—

much greater relative yield strength per relative density when compared to C03. Further testing and theoretical analysis need to be done to verify these results and hypotheses.

The flexure tests were carried out in such a way that not much information was revealed about the relationship between structure and property. Upon analysis of the test procedure, several flaws were revealed. The first of these involved the dependency of the structures' properties on the translation of the unit cell. For example, if the bars were constructed of layers of two unit cells in the *z*-direction (which was the case), the unit cell configuration that placed the most mass on the top and bottom faces of the bar would result in a higher relative strength for a similar relative density. Several more sources of potential error resulted from the modification of the standard three-point flexure test. As mentioned in Sec. 3, the traditionally round supports were replaced with flat ones. The flat support at middle of the bar did not remain level in most tests, creating an uneven force distribution between the two contact points edges between the mobile support and the bent bar. Second, the displacement measurement collected represented the displacement of the mobile support, not the displacement of the middle of the bar.

There were several positive takeaways to be gathered from the flexure tests. The first is the confirmation that the unit cells with the greatest proportion of mass on the top and bottom faces produced the greatest flexural strengths. These structures included C01, H03, C03, and H01. Again, H04 was not included in the results for reasons to be discussed.

The differences between results from the unit cells of H02 and H03 were useful in demonstrating the effects of scaling on a hexagonal cell. H02 is a denser variant of H03, with a smaller central hexagon with a slightly different orientation than H02. Therefore, a preliminary hypothesis that their properties would be proportional to their different densities was reasonable. This was shown to be the case. The relative density ratio from H02 to H03 was 2.03. The ratio of the same cubes' relative flexural strengths was 2.26 for the high case and 2.28 for the low case. Scaling the relative density of similar unit cells appears to produce a near proportional scaling of the relative strength. The bounds of this relationship, in addition to the validity of the proportionality claim, necessitate additional research to confirm the stated hypothesis.

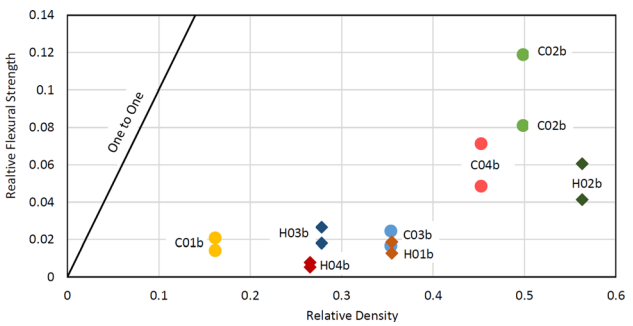

Fig. 13 Summary of results from the first series of flexure tests

Table 7 Second series compression geometries polymer and aluminum

Name	Unit structure	Unit cell dimensions (mm)			Cube dimensions (mm)			Compression face area (mm^2)	Relative density (Netfabb)
		x	*y*	*z*	*x*	*y*	*z*		
Pyra_067		10.00	10.00	6.70	40.11	40.02	26.69	1605.20	0.20
Pyra_100		10.00	10.00	10.00	40.11	40.02	39.95	1605.20	0.15
Pyra_133		10.00	10.00	13.30	40.10	40.00	53.30	1604.00	0.13
Tetra_067		17.30	10.00	6.70	52.10	50.07	26.70	2608.65	0.28
Tetra_100		17.30	10.00	10.00	52.10	50.07	39.90	2608.65	0.22
Tetra_133		17.30	10.00	13.30	52.05	50.03	53.34	2604.06	0.19
Kag_067		12.00	20.80	6.70	60.13	62.37	26.69	3750.31	0.25
Kag_100		12.00	20.80	10.00	60.13	62.37	39.95	3750.31	0.22
Kag_133		12.00	20.80	13.30	60.13	62.37	53.24	3750.31	0.21

In either test, the results of the H04 unit cell should be discarded. This particular unit cell was not effectively implemented in the established structure due to its large size. While the other overall compressive structures contained from 64 to 125 unit cells, the H04 structure contained less than a total of 11 unit cells in the entire structure. As shown in later testing, the obtained results did not represent the characteristics of the H04 unit cell geometry well. Not only that but many of these cells were cut off due to the geometric constraints placed on the overall structure (see Fig. 9), rendering some of the trusses structurally unnecessary and wasting mass. Therefore, the results for the H04 structures should not be considered.

While this testing was useful for observing the relative characteristics of the given unit cells within a geometric constraint, the research would be even more useful had the cells been compared at different relative densities. Had that been the experimental variable, the general performance of the unit cells across multiple relative densities would lead to a range of relative properties, better characterizing the unit cell's effectiveness. These gaps in the preliminary tests resulted in the formulation of the second tests series with additional structures and goals.

5 Second Test Series

5.1 Development of Second Series Unit Cell Structures and Specimen. As stated in Sec. 4.3 for the first series of testing, two significant factors were overlooked during the research. Those included the influence of the total number of unit cells on overall properties (alike H04), and the lack of variety in unit cell construction. The second series of testing was intended to further explore the relation between unit cell and overall relative properties. For the second tests, the basic geometries consisted of only three base unit cells. These base cells were then scaled in the *z*-direction to create a total of three variations of each base cell. These different variations each presented a modified relative density and slight geometric difference to broaden the scope of the trial. Additionally, after the tests of the polymer specimens, one set of cubes intended for compression was additively manufactured in aluminum alloy. The objective was to compare the coherences of the performance with different materials.

The selected base geometries were C03, H04, and a new structure, based on kagome tiling [16]. Kagome has shown promise in lattice structure experimentation [14]. It consists of periodic trihexagonal tiling aligned identically on the top and bottom planes. Nodes of one plane were connected to the immediately adjacent nodes of the opposite plane, see Table 7 for a view of the unit cell. In addition, further research showed structures based on the tiling demonstrated higher relative strength per relative density than C03 [14]. C03 was chosen for continued testing due to its multidirectional functionality, the capability to operate in several directions. H04 was selected to reassess the geometry after inconclusive results during the first test series. All geometries used in the second test series utilized the same 2 mm truss design as was used in the first specimens. Figure 14 shows the three considered unit cells in the second test series.

The specimens were named according to their base geometry and the scale factor. All names take the form of NAME_XXX, where NAME represents the base geometry and XXX represents the scaling factor multiplied by 100. An "A" following the name was used to designate aluminum cubes, while a "b" following the name designates the structure was designed for a flexural test. It should be noted that the geometries were scaled in the *z*-direction only (see Tables 7 and 8). Due to overall size constraints and adherence to the ASTM standards, the scaling factors of the flexure geometries had to be modified from those of the compressive structures. All of the scaling factors of the bending samples are less than one. The pre-existing C03 and H04 geometries from the first test series were renamed respectively to pyramidal or "pyra" (previously C03) and tetragonal or "tetra" (previously H04). These names better represent the

Fig. 14 Unit cells pyra, tetra, and kag considered in the second test series

Table 8 Second series flexure geometries

Name	Unit structure	Unit Cell dimensions (mm)			Bar dimensions (mm)			Support–support distance (mm)	Relative density (Netfabb)
		x	*y*	*z*	*x*	*y*	*z*		
Pyra_050b		10.00	10.00	10.00	190.29	30.00	10.12	69.75	0.23
Pyra_067b		10.00	10.00	13.40	240.20	30.00	13.62	94.70	0.18
Pyra_075b		10.00	10.00	15.00	270.20	30.00	15.02	109.70	0.17
Tetra_050b		10.00	17.30	10.00	189.93	34.82	10.15	69.57	0.33
Tetra_067b		10.00	17.30	13.40	240.01	34.80	13.60	94.61	0.27
Tetra_075b		10.00	17.30	15.00	270.00	34.80	15.01	109.60	0.26
Kag_050b		12.00	20.80	10.00	192.30	41.60	10.10	70.75	0.29
Kag_067b		12.00	20.80	13.40	240.28	41.60	13.40	94.74	0.26
Kag_075b		12.00	20.80	15.00	276.27	41.60	15.00	112.74	0.24

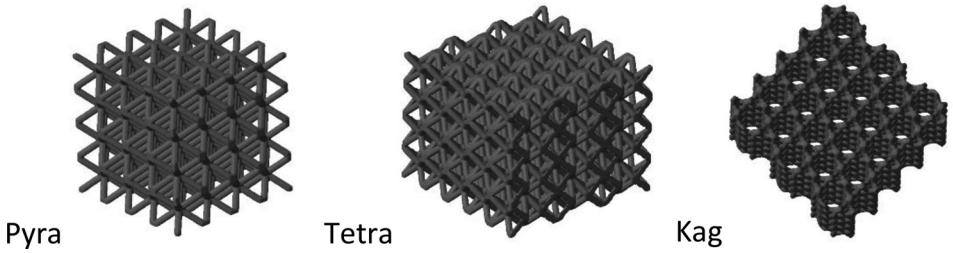

Fig. 15 Compression test cubes pyra, tetra, and kag considered in the second test series

unit cell geometry and help distinguish the samples intended for the second test series from the first test series. This kagome pattern is referred to as simply kagome or "kag" for brevity.

The overall geometry of the compression structures was designed in such a way as to accommodate a whole number of unit cells and to make the unit cells as close to cubic as possible. Additionally, the number of unit cells present in each geometry was kept as consistent as practical. The pyra structure contained 64 cells, while tetra and kagome contained 92. This process resulted in the geometries presented in Fig. 15 and Table 7. The bending specimens were only constrained by the scale factor and the ASTM standards, geometries shown in Table 8.

5.2 Test Results and Calculation. Testing was carried out as described in Sec. 3. Similar to Sec. 4.2, the raw data were not included because of its volume. Instead, the emphasis was on the manipulation of the obtained data to produce the desired results. The focus of this study was to compare the relative properties of the various structures with their relative density. Although, the flexural test method has some sources of potential error as described in Sec. 4.3, it was decided to use the same test procedure for the second test series. Also, the procedure used to calculate the desired information is identical to that used for the first test series. The same value for polymer yield strength determined in the previous tests was used in these calculations.

Unique to the second test series is the inclusion of specimens printed in aluminum. So far, only compressive samples were printed due to financial constraints. The research on the flexural tests will be continued. As mentioned in Sec. 3, the aluminum cubes were not all printed in the same direction[2] (see Fig. 16), but this factor was adjusted for by utilizing directionally dependent yield strengths.

5.2.1 Compression. Results were obtained as in the previous Results and Calculation section (see Sec. 4.2.1) and presented in tabulated and graphical formats. Polymer results are presented in Figs. 17 and 18 and Table 9, while aluminum results are found in Figs. 19 and 20 and Table 10. Unique to the aluminum cubes was the varied cube build direction. Some of the cubes were built with the intended compression direction normal to the print bed, while the rest were built with the intended compression direction parallel to the bed plane. The material yield strength was provided for forces exerted both parallel to the bed plane (275 MPa) and normal to the bed plane (230 MPa). The value for yield strength used for determining the relative yield strength (based on the build direction) can be found in the material yield strength column of Table 10.

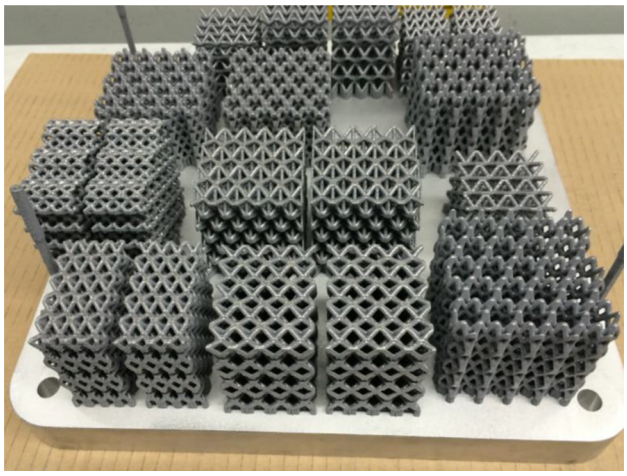

Fig. 16 Aluminum compression test cubes based on the build direction, placed to maximize manufacturing efficiency[3]

[2]Aluminum samples were fabricated by Citim AM, Inc., using an SLM 280 machine.

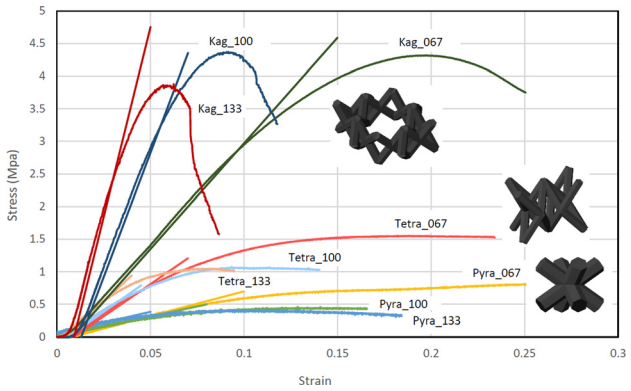

Fig. 17 Compression test results as stress–strain curve of polymer cubes pyra, tetra, and kag with offset curves

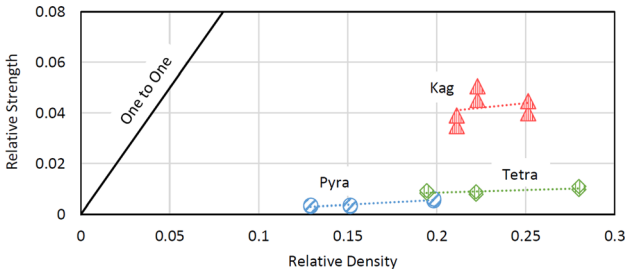

Fig. 18 Summary of results from second series polymer compression tests

5.2.2 Flexure. The procedure for the calculation of the relative flexural strength followed the steps outlined in the first test series (see Sec. 4.2.2). Table 11 and Fig. 21 show calculated and measured results of the flexure test.

5.3 Analysis of Second Test Series Results. The second series of testing yielded much more practical results than the first test series. For each variation of the three basic unit cells, the relationship between relative property and relative density was determined (see Figs. 18, 20 and 21). The results from the three variations for each basic cell geometry created a range of attainable relative density-to-property ratios for each basic structure. While this range of data was not exhaustive, the data obtained may be useful for lattice structure design and application.

Several observations were made from the compression data. The first of these is the much higher relative yield stresses obtained by the kagome structures in comparison to tetra and pyra structures. The range of kagome relative densities overlapped the tetra relative densities, yet the relative yield strengths of the kagome structures were more than twice those of the tetra structures. While all structures were bend-dominated, the kagome-derived lattice exhibited superior property-to-mass performance.

Between the tetra and pyra structures, there existed slight overlap in relative densities. The highest pyra relative density was greater than the lowest tetra relative density. This overlap clearly demonstrated the higher relative yield strengths attainable with the tetra structures. The slope of the trend lines suggested that the tetra structures would generally result in higher yield strengths than the pyra structures except in extreme relative densities. Both polymer and aluminum tests supported this result.

In nearly every geometry group, the yield strength corresponding to the unscaled specimen was lowest, followed by the 1.33 scale, and the 0.67 scale was strongest. The only exception to this trend was the polymer kagome group. These results might seem to contradict the conclusions of the first group of tests, which postulated that the more vertical a truss, the higher is the overall relative yield strength. However, in the first series of testing, no angles below 45 deg between trusses were present. As the angle decreases, the union of two three-dimensional trusses occurs farther away from the drafted point of intersection. This earlier union may have led to increased material at each node, in addition to more supporting material farther away from the node. This reinforcement may assist in resisting the moments caused by compression, essentially strengthening the lattice. While this reinforcement would exist in all nonorthogonal trusses, the low angles present in the 0.67 scaled geometries may have been significant enough for the nodal reinforcement to take noticeable effect. Additionally, it should be noted that the 0.67 specimens had the highest relative densities. This also would have contributed significantly to the trend in scaled geometries.

The pattern of results between scaled specimens was largely consistent for both aluminum and polymer tests. However, the aluminum results were much closer to the unity ratio. The dependence of the lattice structure on material is not an unknown phenomena [48], but further research is necessary to find an explanation or formulate a hypothesis to explain these findings.

Finally, it should be briefly noted that the trend line for each family has a slope that is positive but less than one. This suggests

Table 9 Summary of second series polymer compression results

Name	Unit structure	Relative density (Netfabb)	Yield strength (MPa)	Relative yield strength	
				Low	High
Pyra_067		0.20	0.38	0.005	0.006
Pyra_100		0.15	0.22	0.003	0.004
Pyra_133		0.13	0.22	0.003	0.004
Tetra_067		0.28	0.69	0.010	0.011
Tetra_100		0.22	0.55	0.008	0.009
Tetra_133		0.19	0.59	0.008	0.009
Kag_067		0.25	2.81	0.040	0.045
Kag_100		0.22	3.18	0.045	0.051
Kag_133		0.21	2.45	0.035	0.039
Solid	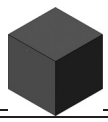	1.00	62.8–70.4	—	—

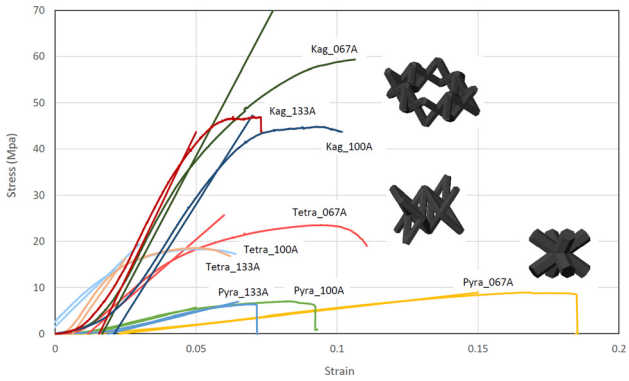

Fig. 19 Compression test results as stress–strain curve of aluminum cubes pyra, tetra, and kag

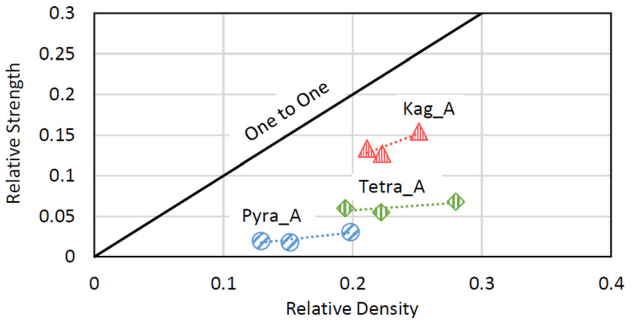

Fig. 20 Summary of results from aluminum cubes compression tests

that the lower the relative density, the more efficient the used material would become. The converse is also suggested to be true. Though the relative density of a structure may be increased and the relative strength increased, the data point would only get farther from the one-to-one ratio.

The flexural testing returned results summarized by Fig. 21. Interestingly, tetra and kagome returned nearly identical results. Both kagome and tetra structures occupied higher relative densities and relative yield strengths than pyra, with the exception of a single point. Unfortunately, due to reasons discussed in Sec. 4.3, these results cannot be taken to fully represent the properties of the tested lattices. However, there is little reason to doubt that the general trends revealed in the flexural tests are valid. For example, it is reasonable to believe that kagome and tetrahedral lattice structures will, in fact, produce a much higher relative flexural strength per relative density than pyra structures.

Table 10 Summary of aluminum compression results

Name	Unit structure	Density (Netfabb)	Material yield strength (MPa)	Measured yield strength (MPa)	Relative yield strength
Pyra_067A		0.20	230	7.09	0.031
Pyra_100A		0.15	275	4.98	0.018
Pyra_133A		0.13	275	5.43	0.020
Tetra_067A		0.28	230	15.68	0.068
Tetra_100A		0.22	230	12.7	0.055
Tetra_133A		0.19	230	13.8	0.060
Kag_067A		0.25	230	35.5	0.154
Kag_100A		0.22	275	34.9	0.127
Kag_133A		0.21	275	36.7	0.133

Table 11 Summary of second series polymer flexure results

				Relative yield strength	
Name	Unit structure	Relative density (Netfabb)	Flexural strength(MPa)	Low	High
Pyra_050b		0.23	1.19	0.011	0.016
Pyra_067b		0.18	0.64	0.006	0.009
Pyra_075b		0.17	0.46	0.004	0.006
Tetra_050b		0.33	5.17	0.047	0.069
Tetra_067b		0.27	2.77	0.025	0.037
Tetra_075b		0.26	1.94	0.018	0.026
Kag_050b		0.29	3.55	0.032	0.047
Kag_067b		0.26	2.07	0.019	0.028
Kag_075b		0.24	1.54	0.014	0.021
Solid		1.00	75–110	—	—

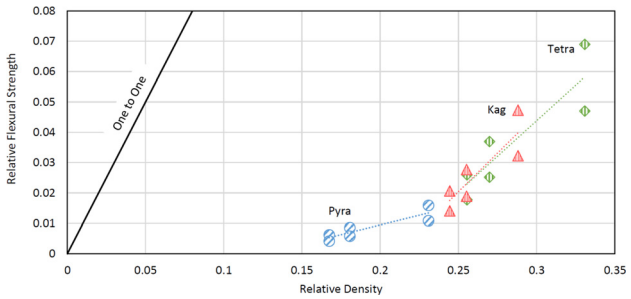

Fig. 21 Summary of second series polymer flexural results

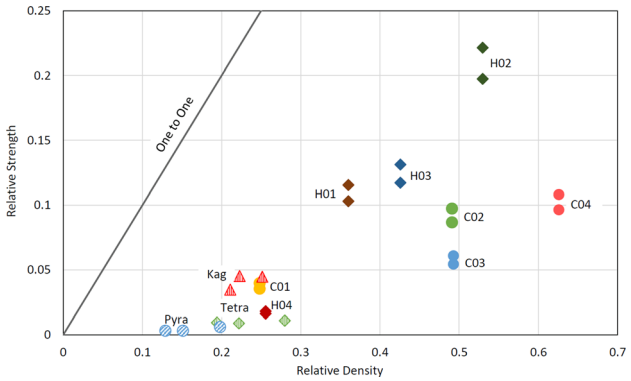

Fig. 22 Summary of compressive test results of polymer cubes from the first and second test series

6 Conclusions

This research yielded several trends in lattice structure geometry–property relations. The first series of testing uncovered the relative properties of several basic lattice structures developed around cubic and hexagonal designs. The results were presented in terms of relative density and relative property, where the relative property was yield strength for compression tests and flexural strength for bend tests. It was found that cells with vertical trusses returned results closest to that of a solid cube, with hexagonal results returning the highest relative yield strengths. The first flexure tests were partially disregarded due to unforeseen difficulties associated with testing periodic lattice structures. However, it was noted that the scaling of relative density resulted in a similar scaling of relative flexural strength.

The second series of testing was designed to more fully explore three selected unit cell geometries and fill gaps in the first tests. The second series incorporated three scaled variants of the three chosen base geometries, for a total of nine specimens. The three chosen structures included a square pyramidal structure, a tetrahedral structure, and a kagome-sourced structure. These tests demonstrated the supremacy of the kagome-derived structure, which was frequently closest to the unity ratio (property of a solid substance). They also demonstrated the practicality of aluminum lattice structures, with relative yield strengths greater than half the relative density. The results of scaling were also presented, with the unscaled unit cells (constructed to be as close to cubic as practical) generally returning the lowest relative yield strength within each base structure group. The specimens scaled by 0.677 returned the highest yield strength, most likely due to their higher relative density and increased material at truss intersections. There was only one exception to this trend—polymer kagome compression. A final graphical comparison of the compressive polymer specimens is presented in Fig. 22. As can be seen, the kagome structure was closest to the solid ratio.

This research served as a preliminary look into the relationship between lattice geometry and relative property. While the research was helpful to build an understanding from basic cells, additional research may proceed in many directions. Directly from this research, additional testing was required to investigate the dependency of structure properties on truss angles within the unit cell. Also, the bounds to the established relative density to relative property ratios (trend lines) within the second trial structures should be explored. Additional topics may include shear testing, compression in multiple directions, tensile testing, etc. Many mechanical properties are yet to be explored. Moreover, more advanced geometries may be tested. The results have also suggested that at a certain point the linear relationship between the relative density and the relative strength may appear to plateau. It is important to further investigate at which point the linear relationship may break down as it relates to the weight and strength of lattice structures.

In addition, the gained experimental results will be merged with the analytical work, which has been done in parallel with ongoing activities. For example, an optimization on a single cubic cell was performed to verify the optimal lattice shape and size within a predefined space by using the SOLIDTHINKING INSPIRE software [49]. Several lattice configurations were analyzed both from a micro level (single unit cell) and a macro level (a simple series of unit cells). Optimization was performed with respect to stiffness and compliance to identify strategic configurations for different kind of load cases.

Finally, case studies may be pursued, implementing the lattice structures in practical applications. It is certain that lattice structures and lightweight design will become one of the key factors in the inevitable acceptance and further utilization of AM technologies as a production tool. Knowledge of optimal lattice configurations from a structural standpoint and well-defined design guidelines will enable design engineers to further reduce weight and increase structural efficiencies when designing for AM.

Acknowledgment

We acknowledge the support of netfabb GmbH by providing free access of a SELECTIVE SPACE STRUCTURES (3S) software license, and Citim AM, Inc., for sponsoring the fabrication of the Aluminum specimens for the experimental tests.

References

[1] Gibson, I., Rosen, D. W., and Stucker, B., 2009, *Additive Manufacturing Technologies: Rapid Prototyping, and Direct Digital Manufacturing*, Springer, New York.
[2] Beyer, C., and Kochan, D., 2013, "Potential for Innovation in Additive Manufacturing," *Pahl/Beitz Engineering Design: Fundamentals of a Successful Product Design Process*, 8th ed., J. Feldhusen, and K.-H. Grote, eds., Springer Vieweg, Berlin/Heidelberg, Germany, pp. 48–98 (in German).
[3] Beyer, C., 2014, "Strategic Implications of Current Trends in Additive Manufacturing," ASME J. Manuf. Sci. Eng., **136**(6), p. 064701.
[4] Huang, Y., Leu, M. C., Mazumder, J., and Donmez, A., 2015, "Additive Manufacturing: Current State, Future Potential, Gaps and Needs, and Recommendations," ASME J. Manuf. Sci. Eng., **137**(1), p. 014001.
[5] Song, X., Pan, Y., and Chen, Y., 2015, "Development of a Low-Cost Parallel Kinematic Machine for Multidirectional Additive Manufacturing," ASME J. Manuf. Sci. Eng., **137**(2), p. 021005.
[6] Wu, D., Rosen, D. W., and Schaefer, D., 2015, "Scalability Planning for Cloud-Based Manufacturing Systems," ASME J. Manuf. Sci. Eng., **137**(4), p. 040911.
[7] Modekurthy, V. P., Liu, X. F., Fletcher, K. K., and Leu, M. C., 2015, "Design and Implementation of a Broker for Cloud Additive Manufacturing Services," ASME J. Manuf. Sci. Eng., **137**(4), p. 040904.
[8] Beyer, C., and Figueroa, D., 2015, "Lattice Structure Implementation and Design Principles," RAPID 2015, Long Beach, CA.
[9] Casadei, A., and Broda, R., Ricardo, Inc., 2008, "Impact of Vehicle Weight Reduction on Fuel Economy for Various Vehicle Architectures," Report No. 2008-04, Project FB769, RD.07/71602.2, The Aluminum Association, Arlington, VA.
[10] Federal Aviation Administration, 2009, "Semi-Annual Launch Report," FAA, Washington DC.
[11] Gibson, L. J., and Ashby, M. F., 1999, *Cellular Solids, Structure and Properties*, 2nd ed., Cambridge University Press, Cambridge, UK.
[12] Ford, C. M., and Gibson, L. J., 1998, "Uniaxial Strength Asymmetry in Cellular Materials: An Analytical Model," Int. J. Mech. Sci., **40**(6), pp. 521–531.

[13] Gibson, L. J., Ashby, M. F., and Harley, B. A., 2010, *Cellular Materials in Nature and Medicine*, Cambridge University Press, Cambridge, UK.
[14] Ashby, M., 2006, "The Properties of Foams and Lattices," Philos. Trans. R. Soc., A, **364**(1838), pp.15–30.
[15] Wadley, H. N., 2006, "Multifunctional Periodic Cellular Metals," Philos. Trans. R. Soc., A, **364**(1838), pp. 31–68.
[16] Moongkhamklang, P., Elzey, D. M., and Wadley, H. N., 2008, "Titanium Matrix Composite Lattice Structures," Composites, Part A, **39**(2), pp. 176–187.
[17] Choi, J., and Chae, T.-S., 2015, "Effective Stiffness and Effective Compressive Yield Strength for Unit-Cell Model of Complex Truss," Int. J. Mech. Mater. Des., **11**(1), pp. 91–110.
[18] Zhang, P., Toman, J., Yu, Y., Biyikli, E., Kirca, M., Chmielus, M., and To, A. C., 2015, "Efficient Design-Optimization of Variable-Density Hexagonal Cellular Structure by Additive Manufacturing: Theory and Validation," ASME J. Manuf. Sci. Eng., **137**(2), p. 021004.
[19] Jeong, N., and Rosen, D. W., 2014, "Microstructure Feature Recognition for Materials Using Surfacelet-Based Methods for Computer-Aided Design-Material Integration," ASME J. Manuf. Sci. Eng., **136**(6), p. 061021.
[20] Yang, L., 2015, "Experimental-Assisted Design Development for an Octahedral Cellular Structure Using Additive Manufacturing," Rapid Prototyping J., **21**(2), pp. 168–176.
[21] Valdevit, L., Jacobsen, A. J., Greer, J. R., and Carter, W. B., 2011, "Protocols for the Optimal Design of Multi-Functional Cellular Structures: From Hypersonics to Micro-Architected Materials," J. Am. Ceram. Soc., **94**(1), pp. 15–34.
[22] Pal, D., Patil, N., Zeng, K., and Stucker, B., 2014, "An Integrated Approach to Additive Manufacturing Simulations Using Physics Based, Coupled Multiscale Process Modeling," ASME J. Manuf. Sci. Eng., **136**(6), p. 061022.
[23] Nelaturi, S., Kim, W., and Kurtoglu, T., 2015, "Manufacturability Feedback and Model Correction for Additive Manufacturing," ASME J. Manuf. Sci. Eng., **137**(2), p. 021015.
[24] Gaynor, A. T., Meisel, N. A., Williams, C. B., and Guest, J. K., 2014, "Multiple-Material Topology Optimization of Compliant Mechanisms Created Via PolyJet Three-Dimensional Printing," ASME J. Manuf. Sci. Eng., **136**(6), p. 061015.
[25] Rua, Y., Muren, R., and Reckinger, S., 2015, "Limitations of Additive Manufacturing on Microfluidic Heat Exchanger Components," ASME J. Manuf. Sci. Eng., **137**(3), p. 034504.
[26] Brant, A. M., Sundaram, M. M., and Kamaraj, A. B., 2015, "Finite Element Simulation of Localized Electrochemical Deposition for Maskless Electrochemical Additive Manufacturing," ASME J. Manuf. Sci. Eng., **137**(1), p. 011018.
[27] Sundaram, M. M., Kamaraj, A. B., and Kumar, V. S., 2015, "Mask-Less Electrochemical Additive Manufacturing: A Feasibility Study," ASME J. Manuf. Sci. Eng., **137**(2), p. 021006.
[28] Wang, H., Chen, Y., and Rosen, D. W., 2005, "A Hybrid Geometric Modeling Method for Large Scale Conformal Cellular Structures," ASME Paper No. DETC2005-85366.
[29] Nguyen, J., Park, S.-I., and Rosen, D. W., 2012, "Cellular Structure Design for Lightweight Components," Innovative Developments in Virtual and Physical Prototyping—5th International Conference on Advanced Research and Rapid Prototyping, pp. 203–210.
[30] Medeiroseså, A., Mello, V. M., RodriguezEchavarria, K., and Covill, D., 2015, "Adaptive Voids: Primal and Dual Adaptive Cellular Structures for Additive Manufacturing," Visual Comput., **31**(6–8), pp. 799–808.
[31] Challapalli, A., and Ju, J., 2014, "Continuum Model for Effective Properties of Orthotropic Octet-Truss Lattice Materials," ASME Paper No. IMECE2014-38925.
[32] Hibbeler, R. C., 2011, *Statics and Mechanics of Materials*, R. C. Hibbeler, ed., Pearson, New York, p. 379.
[33] Masonry Laboratory, 2007, "Masonry Society," University of Wyoming, Laramie, WY.
[34] Total Materia, 2001, "Engineering Stress-Strain Curve: Part One," Total Materia, Zurich, Switzerland.
[35] Instron, 2015, "Flexural Strength," Instron, Norwood, MA.
[36] Netfabb, 2015, "Product Description: netfabb Selective Space Structures (3S)," netfabb GmbH, Parsberg, Germany.
[37] Wikipedia Encyclopedia, 2015, "File Format Description: STL (File Format)," Wikimedia Foundation, Inc., San Francisco, CA.
[38] Wikipedia Encyclopedia, 2015, "File Format Description: Additive Manufacturing File (AMF) Format," Wikimedia Foundation, Inc., San Francisco, CA.
[39] Siraskar, N., Paul, R., and Anand, S., 2015, "Adaptive Slicing in Additive Manufacturing Process Using a Modified Boundary Octree Data Structure," ASME J. Manuf. Sci. Eng., **137**(1), p. 011007.
[40] Stratasys, 2015, "PolyJet Technology," Stratasys, Eden Prairie, MN.
[41] Stratasys, 2015, "Objet30 Pro," Stratasys, Eden Prairie, MN.
[42] Stratasys, 2014, "Polyjet Materials Data Sheet," Stratasys, Eden Prairie, MN.
[43] SLM Solutions GmbH, 2015, "SLM 280 HL," SLM Solutions, Luebeck, Germany.
[44] Gu, D., Chang, F., and Dai, D., 2015, "Selective Laser Melting Additive Manufacturing of Novel Aluminum Based Composites With Multiple Reinforcing Phases," ASME J. Manuf. Sci. Eng., **137**(2), p. 021010.
[45] SLM Solutions GmbH, 2015, "SLM Materials," SLM Solutions, Luebeck, Germany.
[46] SAND.CORe, 2013, "Best Practice Guide for Sandwich Structures in Marine Applications," Coordination Action on Advanced Sandwich Structures in the Transport Industries, Under European Commission Contract No. FP6-506330, SAND.CORe.
[47] Deshpande, V. S., Ashby, M. F., and Fleck, N. A., 2001, "Foam Topology Bending Versus Stretching Dominated Architectures," Acta Mater., **49**(6), pp. 1035–1040.
[48] Moon, S. K., Tan, Y. E., Hwang, J., and Yoon, Y.-J., 2014, "Application of 3D Printing Technology for Designing Light-Weight Unmanned Aerial Vehicle Wing Structures," Int. J. Precis. Eng. Manuf., **1**(3) pp. 223–228.
[49] Vernon, R. A., 2016, "Discovering Optimal Unit Cell Configurations When Designing For Additive Manufacturing Using Lattice Structures," M.S. thesis, CSU, Long Beach.